Diffusion and Melt Viscosity of a Main-Chain Liquid Crystalline Polyether

Elizabeth Hall, Christopher K. Ober,* and Edward J. Kramer

Department of Materials Science and Engineering, Cornell University, Ithaca, New York 14853-1501

Ralph H. Colby and Jeffrey R. Gillmor

Corporate Research Laboratories, Eastman Kodak Company, Rochester, New York 14650-2110

Received January 7, 1993

ABSTRACT: Tracer diffusion of a semiflexible main-chain liquid crystalline polyether was studied using forward recoil spectrometry. Investigation of the temperature dependence of melt diffusion showed that in the nematic region the tracer diffusion coefficient, D^*, was nearly independent of temperature and increased rapidly at the onset of clearing. Similar behavior was observed for the temperature dependence of the melt viscosity. Diffusion coefficients were measured as a function of tracer (M) and matrix (P) molecular weights within the nematic region and as a function of P in the isotropic region. In the nematic, D^* was found to scale as $M^{-1}P^{-2.3}$. A strong P dependence was also found in the isotropic phase. These results suggest a macroscopically aligned system in the nematic state which diffuses via a constraint release type of mechanism and, upon clearing, undergoes a sharp increase in constraining tube diameter.

Introduction

Thermotropic liquid crystalline (LC) polymers are now commercially available because they offer a set of properties unmatched by other structural materials, for example, their capacity to withstand harsh chemical and mechanical environments at high temperatures while maintaining a high strength to weight ratio. LC polymers also continue to generate technological interest because of their response to magnetic and electrical fields and their associated optical properties. The ordered mesophase of LC polymers provides a low melt viscosity for injection molding of parts, as well as capabilities to enhance properties such as nonlinear optical responses. Yet mesophase ordering leads to weaknesses due to poor weld line healing and complex microstructures that result in extremely anisotropic fracture properties. Solutions to these technical problems and an understanding of the way in which the complex microstructures of LC polymers evolve will depend on an understanding of chain dynamics in the mesophase. From a scientific point of view, the dynamics of thermotropic polymers provide largely unexplored and technologically relevant territory for polymer physics.

In this paper we describe studies of main-chain LC polymers consisting of rigid mesogenic cores separated by flexible aliphatic spacers. These polymers are semiflexible chains with self-ordering properties that induce anisotropy in their coil conformation. Compared to rigid rod polymers, these semiflexible thermotropic polymers have a smaller persistence length, 60–300 Å,[1] which is still larger than the typical coil size of a flexible chain polymer. Changes in chain conformation of main-chain nematic polymers with temperature have been examined both theoretically[2] and experimentally.[3,4] Anisotropy in the radius of gyration can be quite large in the nematic mesophase; this anisotropy disappears above the clearing transition. In the nematic mesophase, mesogenic groups align with the nematic director and consequently the radius of gyration is larger parallel to the nematic director than it is perpendicular to the director.

The rheology of LC polymers is known to have certain characteristic features not found in ordinary polymers or in small-molecule liquid crystals.[5-7] For example, melt viscosity in LC polymers will often show a plateau at intermediate shear rates (region II of Figure 1) with shear thinning at both low shear rates (region I) and high shear rates (region III).[5] As the temperature is increased, the viscosity of the LC polymers will first decrease upon formation of the mesophase and then abruptly increase at the clearing transition.[8]

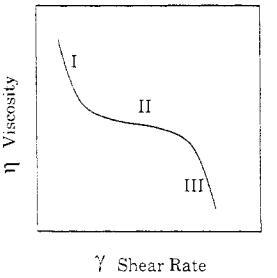

Figure 1. Viscosity versus shear rate behavior of liquid crystalline polymers.

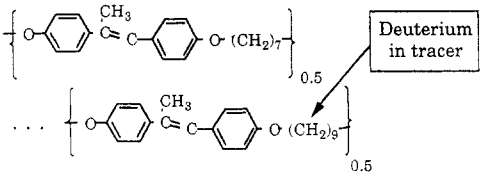

Figure 2. Chemical structure of DHMS-7,9.

This paper describes studies of diffusion and melt viscosity measured for a model main-chain liquid crystalline polyether. The model LC polyether based on 4,4′-dihydroxy-α-methylstilbene and mixed aliphatic spacers (Figure 2) was synthesized in both undeuterated (no hydrogen replaced by deuterium) and partially deuterated forms. A polyether was chosen for our studies to avoid the problem of interchange reactions that would obscure the measurement of diffusion in other LC polymers, especially the more familiar polyesters. The diffusion of trace amounts of the deuterated polymer was measured by determining the depth profile of deuterium after annealing using forward recoil spectrometry.

0024-9297/93/2226-3764$04.00/0

Table I. Dependence of Melt Diffusion Coefficients on Tracer and Matrix Molecular Weight[a]

theory	diffusion coeff	α	β
Rouse	D^*	1	none
constraint release	D^*	1	3
reptation	D^*	2	none
rigid rod	$D_\parallel, D_\perp$	1	none

[a] N.B.: Diffusion scales as $D^* \sim M^{-\alpha}P^{-\beta}$.

Melt diffusion in semiflexible main-chain LC polymers remains an area that has not been studied to date, and no theoretical models are as yet available. We review some models for the diffusion of flexible polymer chains below, as they provide a useful framework for the discussion that follows.

Polymer Chain Diffusion. At temperatures sufficiently far above the glass transition temperature, both viscosity and diffusion are found to exhibit Arrhenius behavior. The apparent activation energies calculated for diffusion (D/T) and viscosity should agree,[9] and in fact they are in very close agreement at high temperature.[10-13]

For flexible polymers that are short enough to be unentangled, the Rouse model is used to describe melt dynamics.[14,15] In this model, drag arises from the Brownian motion of subchain units, each having a monomer friction coefficient, ζ. The total friction of the chain is simply the product $N\zeta$, where N is the degree of polymerization. Substituting this quantity into the Stokes–Einstein relation leads to an expression for the diffusion coefficient, $D = k_BT/N\zeta$, where k_B is the Boltzmann constant and T is the absolute temperature. Thus the Rouse model predicts that $D^* \sim M^{-1}$, where D^* is the tracer diffusion coefficient and M is the molecular weight of the tracer species. The matrix is modeled as a continuum and thus no dependence on matrix molecular weight, P, is predicted. Melt viscosity, η, is directly related to the friction of the chain and a structure factor term[9,16] which leads to $\eta \sim M$ in the Rouse model. For any model that has the temperature dependence of viscosity simply given by the temperature dependence of the friction coefficient, the quantity $\eta D^*/T$ should be independent of temperature.[17]

As polymer chains increase in length, different models are used to account for entanglements, yielding different scaling predictions. The reptation theory of de Gennes[18] predicts a strong dependence of both viscosity and diffusion coefficient on chain length, where $\eta \sim M^3$ (where $M = P$) and $D^* \sim M^{-2}P^0$. The regime between Rouse and reptation, applicable to long chains diffusing into a matrix of shorter chains, was modeled by the constraint release models of Klein[19] and Graessley.[20] In this model, the confining tube undergoes Rouse motion with a jump time determined by reptation of the surrounding chains leading to the proportionality $D^* \sim M^{-1}P^{-3}$. Experimentally, it has been shown that the exponent associated with P is not always equal to 3,[21-23] but generally we expect a power law relationship of the form

$$D^* \sim M^{-\alpha}P^{-\beta} \quad (1)$$

For comparison purposes, the various scaling behaviors are listed in Table I.

Diffusion in Low Molar Mass Nematic Liquid Crystals. In aligned nematic melts, self-diffusion of low molar mass liquid crystals has been found to be anisotropic such that diffusion parallel to the nematic director, $D_\parallel$, is typically faster than diffusion perpendicular to the director, $D_\perp$.[24-26] The anisotropy ratio, $D_\parallel/D_\perp$, tends to be small for nematic liquid crystals. At clearing, the diffusion coefficient in the isotropic state, D_i, is usually approximately equal to the average diffusion coefficient of an unaligned nematic sample, $\langle D \rangle$.[24] Not all liquid crystals have shown this behavior, however; some exhibit faster diffusion in the mesophase than in the isotropic phase, i.e., $D_\parallel > D_\perp > D_i$.[26]

The apparent temperature dependence of dynamics in low molar mass LCs is Arrhenius,[24-26] with some hint of Vogel–Fulcher curvature in one data set.[27] Both $D_\perp$ and $D_\parallel$ show about the same activation energy (E_d). The activation energy in the isotropic phase is equal to, or slightly greater than, E_d in the nematic region.[26,28]

Experimental Section

Diffusion Measurements. Diffusion couples consisted of a base layer (the matrix), 1 μm in thickness, spin-coated onto silicon and a top layer of deuterium-labeled polymer (the tracer), approximately 300 Å thick. The tracer layer was spin-coated onto glass, floated onto water, and picked up by the base layer. Samples designed to measure diffusion at temperatures between the glass transition and melting temperatures used as-spun matrix layers. Samples designed to measure diffusion in the LC or isotropic states used base layers that were annealed in the nematic region prior to adding the tracer layer. Annealing was performed to relieve any possible residual orientation caused by the spin-coating process. Bilayers were diffused in air at temperatures between 25 and 35 °C, in a water bath between 45 and 95 °C, and in silicone oil between 95 and 250 °C. Water and oil baths produced identical D^* values at 95 °C. The FRES technique was used to depth-profile the volume fraction of labeled chains that had diffused into the base layer. The D^* values were obtained from the d-DHMS-7,9 volume fraction versus depth profiles by a curve-fitting procedure. The details of this experiment are provided in a number of earlier publiciations.[29,30]

Shear Viscosity Measurements. Steady-state shear viscosity, η, was measured on a Rheometrics System IV rheometer employing parallel plates 25 or 50 mm in diameter. Samples were molded without applied pressure just above the isotropic transition temperature (T_i). The samples were then analyzed by first heating above T_i and then lowering the temperature to a desired point before starting either (1) a temperature scan at a fixed shear rate or (2) a shear rate scan at a fixed temperature. DHMS-7,9 showed an increase in viscosity at very low shear rates, so that it was not possible to measure a zero shear rate viscosity (see region I of Figure 1). A shear rate of 1 s^{-1} was chosen so that the system was within region II wherein there is little shear rate dependence.

IR Dichroism Measurements. Infrared dichroism measurements of chain orientation were made at Eastman Kodak Co. with the help of W. McKenna and D. Margevich. An attenuated total reflection infrared (ATR-IR) dichroism technique was used on a Bio-Rad FTS-60A spectrophotometer. Polymer was spin-coated on silicon prisms cut at 30 and 45° angles, allowing a theoretical penetration depth of over 1 μm. The thicknesses of DHMS-7,9 for which orientation was measurable (i.e., absorbances parallel to the substrate remained linear) ranged from about 300 to 6000 Å. Unannealed films were measured, as well as films annealed using the same schedule as diffusion sample matrices. The data from the 1570- and 1605-cm^{-1} aromatic stretches were analyzed, and results showed very close agreement.

Synthesis of Materials. The mesogen, 4,4′-dihydroxy-α-methylstilbene (DHMS), was produced by condensation of chloroacetone and phenol in the presence of sulfuric acid according to procedures described previously.[31,32] Polyethers were synthesized using phase transfer catalysis.[32] The mesogen was copolymerized with a 1:1 molar mixture of 1,7-dibromoheptane and 1,9-dibromononane to produce DHMS-7,9. Deuterium-labeled chains were produced by completely substituting an equivalent amount of perdeuterated 1,9-dibromononane for that in the unlabeled copolymer. Details of the synthesis may be found in refs 29 and 32. Purification of the polymer was completed by reprecipitation from chloroform into methanol. Oligomers were removed by dissolving the product in a 5%

Table II. Molecular Weights and Transition Temperatures of DHMS-7,9

species	M_n	M_w	M_w/M_n	T_g (°C)	T_m (°C)	T_{xn} (°C)	T_{ni} (°C)
matrix							
A	2 600	4 900[a]	1.88	12	84	106	163
B	6 400	12 250	1.91	14	89	104	183
C	7 500	15 500	2.10		90	125	194
D	9 200	17 800[a]	1.93	17	90	113	183
E	13 200	23 400	1.77	18	90	119	190
F	16 500	29 000	1.80	21	95	127	200
G	17 100	27 450	1.60		95	127	200
H	26 000	33 500	1.30		95	127	200
I	23 900	37 700	1.58		95	130	196
J	29 200	45 400	1.55		95	130	200
tracer							
K	3 500	7 000	2.00	13	83	101	160
L	7 250	10 900	1.50	13	85	106	181
M	13 400	25 150	1.88	21	88	111	180
N	13 500	29 000	2.10		92	118	187
O	15 100	25 500	1.69	20	89	110	180
P	16 200	26 600	1.64	21	89	113	183
Q	18 700	33 200	1.77		88	110	178

[a] M_w determined by light scattering.

solution of hot toluene, cooling to room temperature, and filtering off the precipitated polymer. Polyethers were fractionated by incrementally lowering the temperature of a 1 wt % toluene solution and removing each precipitated fraction.

Characterization of Materials. Molecular weights were determined by gel permeation chromatography using tetrahydrofuran (THF) at 35 °C as solvent, a 254-nm UV detector, Ultrastyragel columns of 500-, 10^3-, and 10^4-Å pore sizes, and a linear column with mixed pore sizes. Calibration was made with monodisperse polystyrene standards. An independent check on the weight-average molecular weight of DHMS-7,9 using light scattering was performed by T. H. Mourey of Eastman Kodak Co. on a Chromatix KMX-6 instrument.

Thermal transition temperatures were obtained on a DuPont differential scanning calorimeter interfaced with a DuPont 2000 thermal analysis system and on a Perkin-Elmer DSC-2C differential scanning calorimeter. Heating and cooling rates were 20 °C/min.

Mesophases and transitions were first studied optically using a Leitz polarizing microscope equipped with a Mettler FP-82HT hot stage. X-ray scattering experiments used the same hot stage and were performed at the Cornell High Energy Synchrotron Source using focused monochromated radiation of 1.56 Å. Data at a constant temperature were collected on flat film, while dynamic X-ray diffraction data were collected with an OMA III digital detector system. Subsequent data analysis was performed using the software package Semper VI.

Characteristics of the DHMS-7,9 polymer used in this study are listed in Table II. The number-average molecular weight (M_n), weight-average molecular weight (M_w), and polydispersity index (M_w/M_n) are reported for each fraction. The thermal transition temperatures, melting to the intermediate phase (at T_m), the intermediate to nematic transition (T_{xn}), and the clearing transition from nematic to isotropic (T_{ni}), increase with molecular weight and polydispersity.

DHMS-7,9 exhibits a random coil conformation in solution and follows universal calibration. However, in THF at 35 °C, the polymer solution is close to its Θ condition and exhibits two Mark–Houwink coefficients corresponding to two molecular weight regions: below a value of M_w = 35 000, the coefficient is 0.64, while above this value, it is 0.31. Weight-average molecular weights determined from gel permeation chromatography (GPC) calibrated with polystyrene standards were found to be 2 times as large as values measured by light scattering.[33] Molecular weights of samples A and D (Table II) were measured directly by light scattering. The other molecular weights reported here were determined by GPC recalibrated with light scattering data.

Between the melting point T_m and the transition T_{xn}, the polymer exhibits a finely textured, high-viscosity, birefringent phase, which may be a smectic phase or, more likely, a biphase. Certain evidence is strongly suggestive of a smectic phase. The transition T_{xn} is reproducible on heating and cooling, and, as can be seen in Figure 3, little undercooling is observed. Various annealing cycles have been shown by X-ray diffraction analysis to produce different crystalline forms of the polymer that vary in T_m by 20 °C.[34] In each thermal treatment studied, however, the position of T_{xn} is not affected. Between T_m and T_{xn}, the tracer diffusion coefficient increases with temperature, while viscosity decreases with temperature. Percec *et al.*, from whose work DHMS-7,9 was developed, also found an intermediate phase in DHMS-based copolyethers with 9 and 11 carbon spacers.[29] Although this phase was initially identified as smectic, no X-ray studies or other confirming data have been reported.

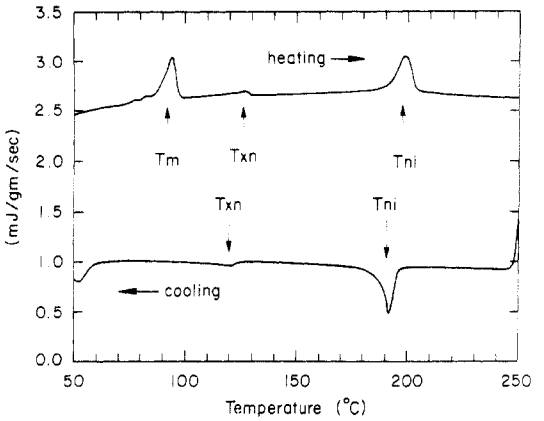

Figure 3. Differential scanning calorimetry of DHMS-7,9 matrix G (Mw = 27 450). The melt transition (at temperature T_m), the intermediate to nematic transition (at temperature T_{xn}), and the nematic to isotropic transition (at temperature T_{ni}) are marked.

Further study of the intermediate phase suggests that it is a biphase. Synchrotron X-ray diffraction data of sample F listed in Table II, as well as other fractions, primarily show nematic diffraction behavior (diffuse ring at 5 Å) between T_m and T_{xn} with very weak low-angle reflections (corresponding to spacings of order ~15 Å) possibly caused by a secondary component. The changes observed in diffusion and rheological behavior could be due either to a small crystalline component or to a smectic cophase, but the nature of the T_{xn} transition suggests that the smectic is the more likely of the two. In summary, we tentatively identify the intermediate phase as a nematic–smectic biphase, and we are working to prove this hypothesis more conclusively.

Above T_{xn}, the polymer is nematic over a temperature range of about 50 °C, until a temperature of approximately 200 °C is reached. From that temperature until 300 °C, the polyether is an isotropic melt and is thermally stable for the times needed to perform the diffusion experiment.

Results

Temperature Dependence of the Diffusion Coefficient. The diffusion behavior of DHMS-7,9 was found to be sensitive to its phase transitions. Changes in slope in plots of tracer diffusion coefficient vs temperature are seen at the melting transition (T_m), the intermediate–nematic transition (T_{xn}), and the clearing transition (T_{ni}) as illustrated in Figure 4 for tracer polymer N diffusing into matrix F.

At temperatures between the glass transition T_g (~20 °C) and the melt transition T_m (~90 °C), the tracer diffusion coefficient increases steadily with temperature T up to T_m. Between T_g and T_m the diffusion was carried out using matrix films that were initially glassy. The noncrystalline nature of the films was confirmed by transmission electron microscopy and thin-film X-ray diffraction measurements. From rheological and synchrotron X-ray observation, it is known that DHMS-7,9 will crystallize at annealing temperatures below T_m and that its rate of crystallization is sensitive to process history. For this reason, the diffusion behavior was examined for the effect of any crystallization during the diffusion process

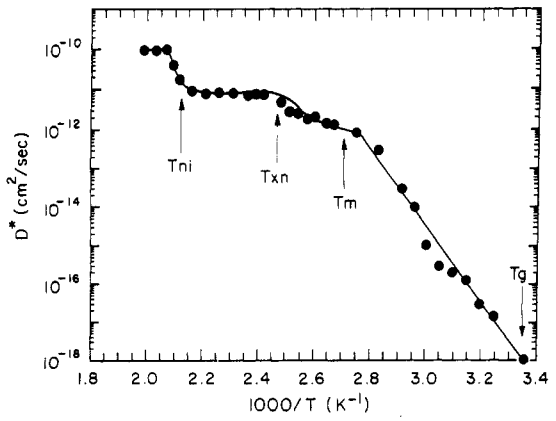

Figure 4. Tracer diffusion coefficient versus inverse temperature for DHMS-7,9 tracer N (M_w = 29 000) and matrix F (M_w = 29 000). Temperatures for the glass transition (T_g), melting (T_m), the intermediate to nematic transition (T_{xn}), and the nematic to isotropic transition (T_{ni}) are indicated with arrows.

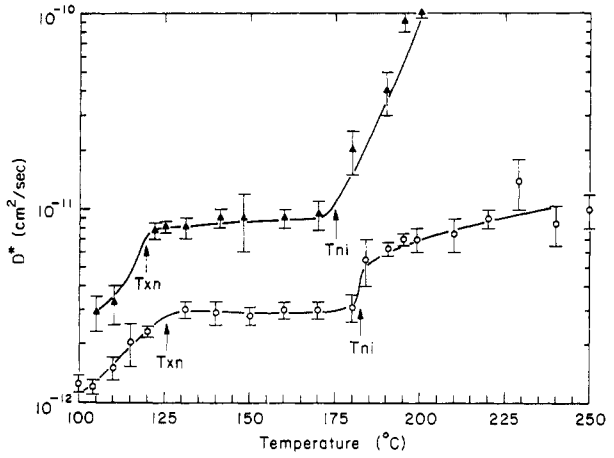

Figure 5. Tracer diffusion coefficient versus temperature of DHMS-7,9 for tracer N (M_w = 29 000) in matrix C (M_w = 15 500) (triangles) and matrix H (M_2 = 33 500) (circles). The intermediate to nematic transition temperature (T_{xn}) and the nematic to isotropic transition temperature (T_{ni}) are marked for each sample.

by diffusing samples at three different times—up to 3 months for samples diffused at room temperature. The diffusion coefficient remained consistent between the samples at each temperature, attesting to the minimal effect of sample history and the Fickian character of the diffusion. The data were averaged to produce the curve shown in Figure 4.

Within the intermediate phase, the diffusion coefficient continues to increase with temperature. In the nematic phase, however, the temperature dependence weakens dramatically so that D^* is effectively independent of T within experimental error. Results of D^* vs T above T_m are shown in Figure 5 for two different molecular weight matrices of DHMS-7,9. These were matrices of fractions C and H, into which were diffused tracer N (sample properties listed in Table II). Both sets of data showed D^* increasing with temperature, prior to formation of the nematic mesophase, whereupon there was a sharp change in slope and D^* became almost independent of T. At the onset of clearing, D^* again increased rapidly, particularly for the diffusion into the lower molecular weight matrix.

Increasing the matrix molecular weight of DHMS-7,9 decreases the magnitude of D^* in the "nematic plateau" region of the D^* vs T curve at a constant tracer molecular weight (N) as can be seen in Figures 4 and 5. The diffusion coefficient decreases with increasing molecular weight, so that in the nematic phase $D^*_C > D^*_F > D^*_H$. In each case,

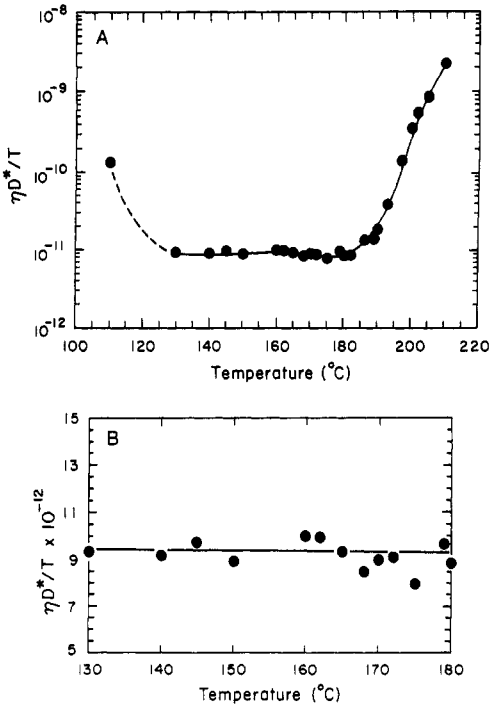

Figure 6. (A) Product of viscosity, tracer diffusion coefficient, and inverse temperature, $\eta D^*/T$, versus temperature (M_w = 29 000). (B) Product of viscosity, the tracer diffusion coefficient, and inverse temperature, $\eta D^*/T$, within the nematic region.

there are abrupt changes in slope at T_{xn} and T_{ni}. Samples of narrow polydispersity such as matrix H showed sharper changes in slope at transitions than did samples with larger M_w/M_n such as matrix C.

To gain further understanding of the nature of the increase in diffusion rate at the clearing transition, we needed to compare self-diffusion results with melt viscosity data. Measurement of polymer self-diffusion, as opposed to the more general measure of tracer diffusion, requires that the molecular weights of the tracer and matrix materials be as closely matched as possible. In polydisperse samples, diffusion scales as the weight-average molecular weight;[35] thus fractions F and N were used for the diffusion bilayers, and fraction F was used for the viscosity measurements. DHMS-7,9 showed a decrease in viscosity with increasing temperature in the intermediate region, a nearly constant viscosity in the nematic phase, and then a sharp increase in viscosity upon clearing. The temperature dependencies of both diffusion and shear viscosity of ordinary flexible polymers are such that $\eta D^*/T$ is nearly independent of temperature.[16,17] In contrast, $\eta D^*/T$ for DHMS-7,9 shows a significant T dependence above T_{ni} and below T_{xn}, as can be seen in Figure 6A. Within experimental error, $\eta D^*/T$ shows no temperature dependence in the nematic phase, as can be seen in Figure 6B.

Molecular Weight Dependence of LC Polymer Diffusion. The dependence of the tracer diffusion coefficient on molecular weight was measured at two temperatures in the nematic regime of the matrix—the first temperature, 130 °C, was just above T_{xn}, and the second, 150 °C, was situated in the middle of the nematic range. Diffusion coefficients are plotted in Figure 7 against the weight-average molecular weight (M) of the tracer polymer.[35] The power law dependence of tracer diffusion coefficient D^* on M is given in terms of the exponent α with a confidence interval of 95% (see eq 1). For samples using matrix G annealed at 130 °C, D^* decreases as $M^{-\alpha}$, where $\alpha = 0.87 \pm 0.58$ (95%). Using matrix I and 150 °C as the annealing temperature, D^* decreases as $M^{-\alpha}$, where

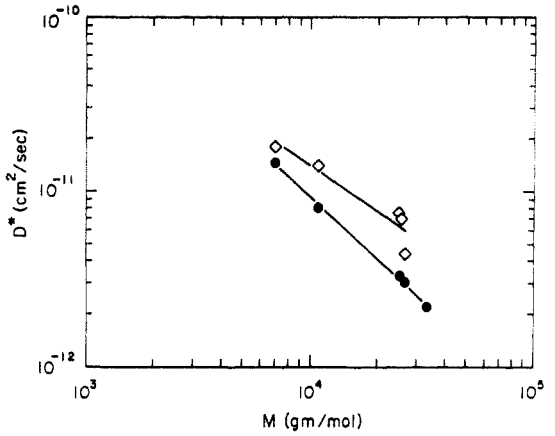

Figure 7. Tracer diffusion coefficient vs the weight-average molecular weight of tracer polymer (M) in the nematic phase for two different matrices: matrix G (M_w = 27 450) (diamonds) and matrix I (M_w = 37 700) (filled circles).

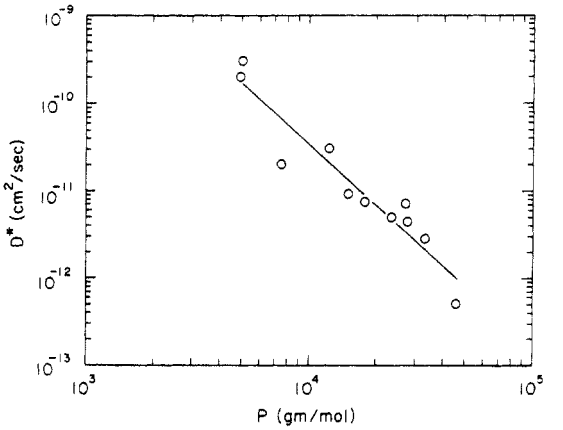

Figure 8. Tracer diffusion coefficient vs the weight-average molecular weight of matrix polymer (P) in the nematic phase for tracer N (M_w = 29 000).

α = 1.18 ± 0.12 (95%). If all these data are pooled, an overall α = 1.03 ± 0.42 (95%) is obtained.

The tracer diffusion coefficient D^* for a given tracer polymer depends strongly on the weight-average matrix molecular weight, P. As shown in Figure 8 for the nematic mesophase, D^* decreases approximately as $P^{-\beta}$, where β = 2.31 ± 0.57 (95%), for tracer N and an annealing temperature of either 130 or 150 °C. This β value is not an artifact of the use of a relatively long tracer, a consideration since the molecular weight of the tracer lies in the middle of the molecular weight range of the matrices used. Indeed, when the low molecular weight tracer K is used and diffused into matrices all of which are higher in molecular weight, the same strong P dependence is observed.

The β value is similarly large in the isotropic phase. Using tracer Q and an annealing temperature of 195 °C, D^* decreases approximately as $P^{-\beta}$, where β = 2.5, as shown in Figure 9. This number should be considered as an upper bound. One reason is that D^* increases with T in the isotropic phase at a rate that is different for each sample; thus it is not meaningful to fix an annealing temperature with respect to T_{ni}. Instead, we must choose a single annealing temperature, despite the variation in T_{ni} between samples. The temperature, 195 °C, was chosen to allow an adequate range of molecular weights to be used, although it is not an optimal temperature for the higher molecular weights. Nonetheless, the data in Figures 5 and 9 clearly point to a strong P dependence in the isotropic phase.

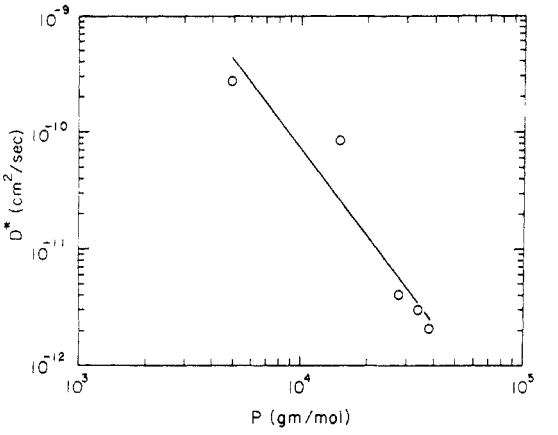

Figure 9. Tracer diffusion coefficient vs the weight-average molecular weight of matrix polymer (P) in the isotropic phase for tracer Q (M_w = 33 200).

Discussion

The most striking characteristic of DHMS-7,9 is the temperature dependence of its tracer diffusion coefficient. The chain dynamics are dramatically affected by phase transitions. There is little temperature sensitivity of D^* or $\eta D^*/T$ in the nematic phase, yet $\eta D^*/T$ is a strong function of temperature both in the intermediate phase and in the nematic–isotropic biphase. This behavior is in contrast to comparable data obtained for (i) side-chain LC polymers where the slope of D vs T is insensitive to phase transitions[36,37] and (ii) ordinary flexible polymers where $\eta D^*/T$ is insensitive to T.[17]

At temperatures between the glass transition temperature T_g and the melting temperature T_m, the diffusion behavior of DHMS-7,9 superficially resembles that of an amorphous, flexible chain polymer. The tracer diffusion coefficient D^* increases steadily with temperature T up to T_m, with an apparent activation energy (E_d) of 46 ± 4 kcal/mol (95%). Crystallinity can be estimated from X-ray diffraction data, and based on the relative areas of the crystalline and nematic/amorphous peaks, the crystallinity is no higher than 15% for any of the heat treatment schedules used.

Within the nematic phase, the apparent activation energy drops sharply. Sample C in Figure 5 showed an E_d = 4.2 ± 3.3 kcal/mol (95%), and sample H showed an E_d = 0.3 ± 0.6 kcal/mol (95%) in the nematic phase. To determine whether this low activation energy is a general feature of nematic main-chain polymers, polyethers with another mesogenic group were synthesized and tested. 2,2′-Dimethyl-4,4′-dihydroxyazoxybenzene (DMAz) was chosen, and two copolymers were made: an analogous mixed spacer polyether (DMAz-7,9) and a mixed mesogen polyether with a single length of spacer (S8Z2-9). DMAz-7,9 was prepared with DMAz and equimolar amounts of dibromononane and dibromoheptane; only a single nematic mesophase was observed.[38] S8Z2-9 was prepared using 80% DHMS and 20% DMAz linked with nonane spacers; both a nematic and an intermediate phase were observed.[37] FRES measurements of D^* vs T showed qualitatively similar changes in slope at phase transitions, as can be seen in Figure 10. Furthermore, the same plateau in slope within the nematic region was observed with an E_d for DMAz-7,9 of 3.4 ± 3.8 kcal/mol (95%) and an E_d for S8Z2-9 of 3.2 ± 1.6 kcal/mol (95%). Samples with higher polydispersity index such as DHMS-7,9 sample C and S8Z2-9 generally showed higher E_d values, an effect that may be caused in part by wide biphasic regions at the end points of the nematic region. In conclusion, low activation

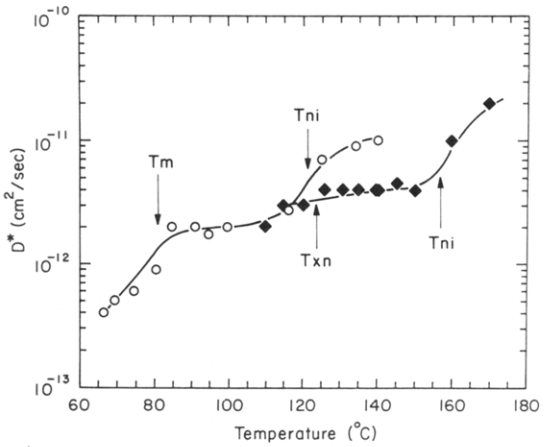

Figure 10. Tracer diffusion coefficient versus temperature of DMAz-7,9 and S8Z2-9 Data are taken from refs 37 and 38. The melting transition temperature is shown for DMAz-7,9 (circles) and the intermediate to nematic transition temperature (T_{xn}) for S8Z2-9 (diamonds). The nematic to isotropic transition temperature (T_{ni}) is marked for both samples.

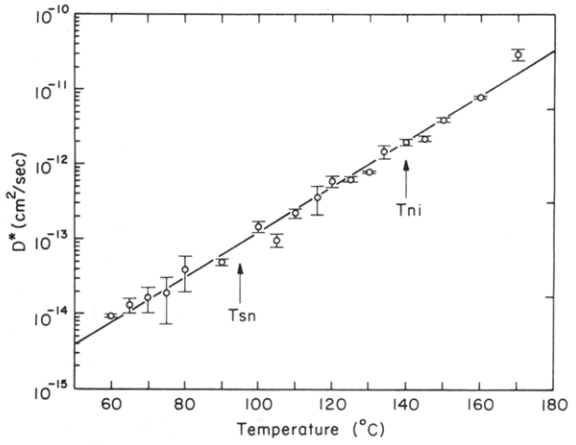

Figure 11. Tracer diffusion coefficient versus temperature of a side-chain liquid crystalline polymer. Data are taken from refs 37 and 38. The smectic to nematic transition temperature (T_{sn}) and the nematic to isotropic transition temperature (T_{ni}) are marked.

energy is a general characteristic of main-chain LC polymers in their nematic phase.

For main-chain systems, the backbone conformation is strongly affected by the nematic ordering of the mesogens. In contrast, a side-chain LC polymer, poly[4-[[6-(methacryloyloxy)hexyl]oxy]-4′-methoxyazobenzene] (PMAM), based on a methacrylate backbone and pendant azobenzene moieties showed a single activation energy across smectic, nematic, and isotropic regions of 20 ± 2 kcal/mol as can be seen in Figure 11.[36,38] Side-chain systems have been shown to have random-coil conformations of their backbone in the nematic phase[39] in contrast to the more extended chain conformations of nematic main-chain LC polymers.[3,4] This backbone conformation plays a large role in chain dynamics. In main-chain nematic polymers chain conformation changes dramatically on clearing, and thus diffusion is very sensitive to clearing (see Figures 4, 5, and 10).

Interestingly, the temperature dependence of diffusion of main-chain polymers is reminiscent of low molar mass LCs in an aligned nematic melt. An increase in diffusion coefficient upon clearing is characteristic of the behavior of the perpendicular component of the diffusion coefficient tensor ($D_\perp$) of low molar mass LCs near the clearing transition. For these low molar mass LCs, the nematic

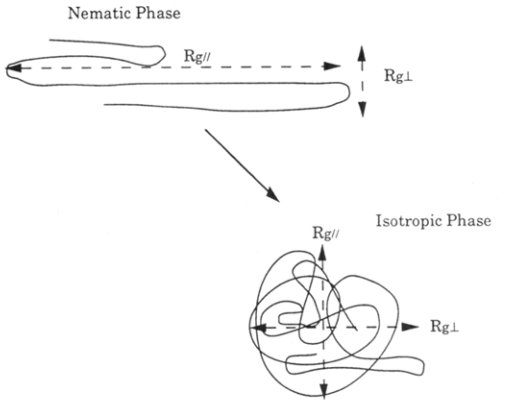

Figure 12. Changes in coil anisotropy resulting from the nematic to isotropic transition.

Figure 13. Entanglement geometry in the nematic mesophase.

directors align with the applied field, so that $D_\perp$ corresponds to the diffusion perpendicular to both director and applied field. The parallel component ($D\|$) typically shows a decrease upon clearing.[24] The data in Figures 4, 5, and 10 are therefore suggestive of a system where only $D_\perp$ and D_i are being observed and the polymer chain conformation is changing at the nematic to isotropic transition as shown in Figure 12.

Evidence for macroscopic alignment of the main-chain LC polymer chains within the film is provided by IR dichroism measurements and electron diffraction observations. Orientation measurements on DHMS-7,9 films annealed in the nematic region using ATR-IR dichroism indicate that the polymer chains, on average, are aligned with the nematic directors parallel to the plane of the substrate. The same measurements on the side-chain polymer, PMAM, annealed in the nematic region showed no evidence of chain alignment within the film. Electron diffraction of thin films of DHMS-7,9 held on a copper grid showed a set of arcs randomly distributed in the plane as the sample was moved across the beam spot. No areas of homeotropic alignment were observed. These observations provide a picture of a main-chain LC polymer film comprised of domains, randomly oriented with respect to one another, but with the directors lying approximately within the plane of the film. The D^* measured by the FRES technique should thus be a good approximation of $D_\perp$ for the main-chain polyethers and of an average D for PMAM.

Tracer diffusion measurements in the nematic and isotropic phases show a strong P dependence, suggesting a mechanism of constraint release (see Table I), which may be rationalized using a simple extension of the constraint release model. In the nematic phase, the static configuration of the main-chain LC polymer may be imagined to be a rigid rod with hairpins,[2,40] as shown in Figure 12, with the additional feature that the rigid rod has Rouse modes due to the flexible spacers between mesogens. These Rouse modes are highly anisotropic, however. The chain is free to move by Rouse-like motions parallel to the director, but in the perpendicular direction, the chain is effectively an assembly of short rigid rods connected by springs and oriented roughly parallel to the director as shown in Figure 13. Doi and Edwards[14] developed a reptation model for a semidilute solution of

Table III. Apparent Activation Energies of Nematic Low Molar Mass and Polymeric Liquid Crystals[a]

liquid crystal	$E_{d\perp}$ (kcal/mol)	$E_{d\parallel}$ (kcal/mol)	E_i (kcal/mol)	ref
p-azoxyanisole[b]	3.5 ± 0.3	2.7 ± 0.1	4.2	24
p-azoxyanisole[c]	8.6	8.1	9.9	26
p,p'-bis(heptyloxy)azoxybenzene[d]	4.7	4.5	8.3	26
p-(methoxybenzylidene)-*p'*-butylaniline[e]	7.6	5.0	7.9	26
p-(methoxybenzylidene)-*p'*-butylaniline with deuterated aromatic rings[f]	4.5 ± 0.2	4.1 ± 0.4	6.9 ± 0.6	24
DHMS-7,9 (matrix C, tracer N)	4.2 ± 3.3			this work
DHMS-7,9 (matrix F, tracer N)	2.8 ± 2.3			this work
DHMS-7,9 (matrix H, tracer N)	0.3 ± 0.6			this work
DMAz-7,9	3.4 ± 3.8			38
S8Z2-9	3.2 ± 1.6			37
PMAM[g]		E_d = 20 ± 1.6		this work

[a] Error calculated as a 95% confidence interval for the polymer data. Expected values range from 0 to (E_d + error value). Other error data taken from the literature where available. [b] PAA. See Table 3 in ref 26. [c] PAA. See Table 1, ref 24. [d] HpAB, a homolog of the PAA series with six carbons in the flexible chain ends. See Table 1, ref 26. [e] MBBA, E values calculated from data in Figure 5, ref 26. [f] DMBBA. See Table in ref 24. [g] Side-chain polymer. E_d calculated from data of Figure 10.

rigid rods and found $D_\parallel$ to be virtually identical to its value in dilute solution but $D_\perp$ to be equal to zero. In the melt where motion of the matrix chains is prevented, we expect the tracer chain to behave similarly to the Doi–Edwards rods. However, constraint release processes should enable diffusion in the perpendicular direction to occur.

Constraint release presumably occurs by a Rouse-like motion of the surrounding tube, as it does in the constraint release models for flexible polymers developed by Klein[19] and Graessley.[20] This idea leads to a diffusion coefficient in the perpendicular direction:

$$D_\perp \approx \frac{a^2 N_e}{12 N \tau_w} \tag{2}$$

where N is the degree of polymerization of the tracer, N_e is the number of monomers between constraints on the diffusing chain, τ_w is a waiting time for diffusion away from one of these matrix constraints, and a is the tube diameter. The fastest mode of motion for the surrounding constraints is a Rouse motion parallel to the director, which produces a waiting time τ_w equal to the longest Rouse relaxation time for the parallel motions $\tau_\parallel$; viz.

$$\tau_w \approx \tau_\parallel \sim P^2 \tag{3}$$

Thus the diffusion coefficient perpendicular to the director scales as

$$D_\perp \sim N^{-1} P^{-2} \tag{4}$$

a dependence which is quite similar to the behavior we observe experimentally.

The tube diameter a and N_e in the nematic melt are expected to be rather small as a result of the nearly rodlike conformation of the tracer chain. In contrast, we expect the tube diameter and N_e ($\sim a^2$) in the isotropic state to be considerably larger. Thus the increase in the magnitude of measured tracer diffusion coefficient from the nematic to the isotropic state is explained qualitatively by the increase in tube diameter accompanying this transition.

This model is also consistent with the weak temperature dependence of D^* in the nematic phase. We expect the temperature dependence of D^* to follow the temperature dependence of the surrounding matrix chains diffusing parallel to the director. Since little change in chain conformation is required for diffusion along the director axis, $D^*(T)$ in LC polymers should be similar to $D_\parallel(T)$ in low molar mass liquid crystals. Literature data support this hypothesis; low molar mass liquid crystals in their nematic phase have E_d values of the same order of magnitude as our LC polymers in their nematic phase. Table III lists literature values for apparent activation energies for self-diffusion in low molar mass nematic liquid crystals with chemical structures similar to DHMS and DMAz.

In the isotropic state, on the other hand, the diffusing matrix chains are random coils and the matrix chain diffusion controlling τ_w should reflect the fact that many conformational changes are necessary for matrix chain diffusion, thus leading to a larger temperature dependence.

We should comment on our hypothesis that the constraint release mechanism controls the tracer diffusion in both the nematic and isotropic states of DHMS-7,9, regardless of the molecular weight of the tracer and the matrix. Diffusion in mixtures of monodisperse polystyrenes (PS) show that constraint release for highly entangled PS is only observed when the matrix molecular weight is well below that of the tracer. However, diffusion in mixtures of polydisperse poly(xylenyl ether) (PXE) exhibited constraint release scaling even for a relatively low M_w tracer (19 000) diffusing into a high molecular weight matrix (M_w = 70 000).[41] We believe this dominance of the constraint release mechanism is a feature of polydispersity and we tentatively ascribe the apparent constraint release scaling we observe in DHMS-7,9 to a similar cause.

Finally, we note that our constraint release model can also explain the difference in diffusion behavior between the main-chain nematic LC polymers, which show little temperature dependence of D^* in the nematic phase and an increase in the value of D^* in the isotropic phase, and the side-chain nematic LC polymer, which showed nearly the same temperature dependence of D^* in both the LC and isotropic states. In the latter case while the mesogens on the side chain align parallel to the director, the polymer backbone conformation remains a random coil throughout the nematic range. Hence little difference in diffusion (i.e., the constraint release) mechaism is expected in the nematic and isotropic states since the constraint on diffusion that matters is the constraint on the backbone motion. Conversely, because the backbone conformation changes markedly between the nematic and the isotropic phase of the main-chain LC polymers, diffusion must be expected to change dramatically, as we observed.

Conclusions

Diffusion of main-chain liquid crystalline polymers was found to be highly sensitive to phase transitions due to strong chain ordering in the mesophase. Diffusion coefficients of DHMS-7,9 measured by forward recoil spectrometery are measurements of $D_\perp$ due to the self-ordering

behavior of the nematic phase with director parallel to the substrate in the thin-film geometry of the experiment. Measured diffusion coefficients show the behavior $D_{\parallel} > D_{\perp}$. A weak temperature dependence of D^* in the nematic phase, with activation energies on the order of those for low molar mass liquid crystals, was found to be characteristic of these main-chain LC polymers. Within the molecular weight range available, the tracer diffusion coefficient D^* scales as $M^{-1}P^{-2.3}$ in the nematic region. This scaling may be interpreted in terms of a constraint release mechanism for diffusion perpendicular to the nematic director. The model also provides insight into the low activation energies observed in the nematic phase.

Acknowledgment. The authors would like to acknowledge support by the National Science Foundation, both for a direct grant and for use of the facilities of the Materials Science Center, and additional financial support by Eastman Kodak Co. G. Galli (Pisa) is acknowledged for his work synthesizing the side-chain polymers. Drs. Thomas Mourey, William McKenna, and Douglas Margevich (Kodak) are thanked for their assistance with molecular weight and IR dichroism measurements, respectively.

References and Notes

(1) Brelsford, G. L.; Krigbaum, W. R. In *Liquid Crystallinity in Polymers*; Ciferri, A., Ed.; VCH Publishers: New York, 1991; Chapter 2.
(2) Williams, R. M.; Warner, M. *J. Phys. (Paris)* **1990**, *51*, 317.
(3) D'Allest, J. F.; Maissa, P.; ten Bosch, A.; Sixou, P.; Blumstein, A.; Blumstein, R.; Teixeira, J.; Noirez, L. *Phys. Rev. Lett.* **1988**, *61*, 2562.
(4) D'Allest, J. F.; Sixou, P.; Blumstein, A.; Blumstein, R.; Teixeira, J.; Noirez, L. *Mol. Cryst. Liq. Cryst.* **1988**, *155*, 581.
(5) Onogi, S.; Asada, T. In *Rheology*; Astarita, G., Marrucci, G., Nicolais, L., Eds.; Plenum Press: New York, 1980; Vol. 1.
(6) Marrucci, G.; Grizzuti, N. *Makromol. Chem., Macromol. Symp.* **1991**, *48/49*, 181.
(7) Wissbrun, K. F. *Br. Polym. J.* **1980**, *12*, 163.
(8) Blumstein, A.; Thomas, O.; Kumar, S. *J. Polym. Sci., Polym. Phys. Ed.* **1986**, *24*, 27.
(9) Berry, G.; Fox, A. *Adv. Polym. Sci.* **1968**, *5*, 261.
(10) Green, P. F.; Kramer, E. J. *J. Mater. Res.* **1986**, *1*, 202.
(11) Nemoto, N.; Landry, M. R.; Icksam, N.; Yu, H. *Polym. Commun.* **1984**, *25*, 141.
(12) Tirrell, M. *Rubber Chem. Technol.* **1984**, *57*, 523.
(13) Bartels, C. R.; Crist, B.; Graessley, W. W. *Macromolecules* **1984**, *17*, 2702.
(14) Doi, M.; Edwards, S. F. *The Theory of Polymer Dynamics*; Clarendon Press: Oxford, 1986.
(15) Rouse, P. E. *J. Chem. Phys.* **1953**, *21*, 1272.
(16) Bueche, F.; Cashin, W. M.; Debye, P. *J. Chem. Phys.* **1952**, *20*, 1956.
(17) Pearson, D. S.; Ver Strate, G.; von Meerwall, E.; Schilling, F. C. *Macromolecules* **1987**, *20*, 1133.
(18) de Gennes, P.-G. *Scaling Concepts in Polymer Physics*; Cornell University Press: Ithaca, NY, 1979.
(19) Klein, J. *Macromolecules* **1978**, *11*, 582.
(20) Graessley, W. W. *Adv. Polym. Sci.* **1982**, *47*, 67.
(21) Lodge, T. P.; Rotstein, N. A.; Prager, S. In *Advances in Chemical Physics*; Prigogine, I., Rice, S. A., Eds.; John Wiley & Sons, Inc.: New York, 1990; Vol. LXXIX.
(22) Shull, K. R.; Kramer, E. J.; Hadziioannou, G.; Antonietti, M.; Sillescu, H. *Macromolecules* **1988**, *21*, 2578.
(23) Green, P. F.; Russell, T. P.; Jérôme, R.; Granville, M. *Macromolecules* **1988**, *21*, 3266.
(24) Kruger, G. J. *Phys. Rep.* **1982**, *82*, 229.
(25) Moscicki, J. K.; Shin, Y. K.; Freed, J. H. In *EPR Imaging and In Vivo EPR*; Easton, G. F., Easton, S. S., Ohno, K., Eds.; CRC Press: Boca Raton, FL, 1991; Chapter 19.
(26) Noack, F. *Mol. Cryst. Liq. Cryst.* **1984**, *113*, 247.
(27) Demus, D.; Hauser, A.; Keil, M.; Wedler, W. *Mol. Cryst. Liq. Cryst.* **1990**, *191*, 153.
(28) Certain low molar mass liquid crystals will show exception to the general trend whereby $E_{d\parallel}$ and $E_{d\perp}$ are not equal and hence $D_{\parallel}/D_{\perp}$ exhibits a temperature dependence.
(29) Angelopoulos, E. H.; Ober, C. K.; Kramer, E. J. *Polym. Mater. Sci. Eng.* **1990**, *63*, 450.
(30) Green, P. F.; Mills, P. J.; Palmstrøm, C. J.; Mayer, J. W.; Kramer, E. J. *Phys. Rev. Lett.* **1984**, *53*, 2145. Green, P. F.; Mills, P. J.; Kramer, E. J. *Polymer* **1986**, *27*, 1063.
(31) Zaheer, S. H.; Singh, B.; Bhushan, B.; Bhargava, P. M.; Kacker, I. K.; Ramachandran, K.; Sastri, D. N.; Rao, N. S. *J. Chem. Soc.* **1954**, *94*, 3360.
(32) Percec, V.; Nava, H.; Jonsson, H. *J. Polym. Sci., Polym. Chem. Ed.* **1987**, *25*, 1943.
(33) Mourey, T. Eastman Kodak Co., private communication.
(34) For example, DHMS-7,9 that is first cleared and then held at 98 °C for 1.5 h will show *d*-spacings of 4 and 5.7 Å and a T_m = 93 °C, while the same material held at 50 °C for 16 h and then at 98 °C for 3 days shows *d*-spacings of 4, 5, 5.7, and 11 Å and a T_m = 113 °C. These samples show markedly different rheological responses as well.
(35) Mills, P. J.; Green, P. F; Palmstrøm, C. J.; Kramer, E. J. *Appl. Phys. Lett.* **1984**, *45*, 957.
(36) Colby, R. H., Gillmor, J. R., Galli, G.; Laus, M.; Ober, C. K.; Hall, E. *Liq. Cryst.* **1993**, *13*, 233.
(37) Hall, E.; Ober, C. K.; Kramer, E. J.; Colby, R. H.; Gillmor, J. R.; Galli, G. *Complex Fluids, Mater. Res. Soc. Symp. Proc.* **1992**, *248*, 113.
(38) Hall, E.; Ober, C. K.; Galli, G. *Liq. Cryst.*, submitted.
(39) Noirez, L.; Moussa, F.; Cotton, J. P.; Keller, P.; Pépy, G. *J. Stat. Phys.* **1991**, *62* (5/6), 997.
(40) de Gennes, P.-G. In *Polymer Liquid Crystals*; Ciferri, A., Krigbaum, W. R., Meyer, R. B., Eds.; Academic Press: New York, 1982.
(41) Composto, R. J.; Kramer, E. J.; White, D. M. *Macromolecules* **1992**, *25*, 4167.